

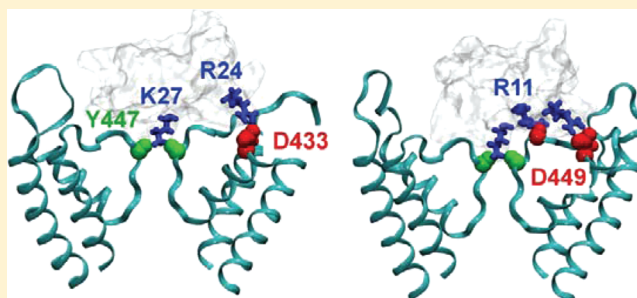
# Engineering a Potent and Specific Blocker of Voltage-Gated Potassium Channel Kv1.3, a Target for Autoimmune Diseases

Rong Chen\* and Shin-Ho Chung

Research School of Biology, Australian National University, Canberra, ACT 0200, Australia

## Supporting Information

**ABSTRACT:** A polypeptide toxin extracted from scorpion venom, OSK1, is modified such that its potency is drastically enhanced in blocking one class of voltage-gated potassium channels, Kv1.3, which is a pharmacological target for immunosuppressive therapy. The bound complex of Kv1.3 and OSK1 reveals that one lysine residue of the toxin is in the proximity of another lysine residue on the external vestibule of the channel, just outside of the selectivity filter. This unfavorable electrostatic interaction is eliminated by interchanging the positions of two amino acids in the toxin. The potentials of mean force of the wild-type and mutant OSK1 bound to Kv1.1–Kv1.3 channels are constructed using molecular dynamics, and the half-maximal inhibitory concentration ( $IC_{50}$ ) of each toxin–channel complex is computed. We show that the  $IC_{50}$  values predicted for three toxins and three channels match closely with experiment. Kv1.3 is half-blocked by 0.2 pM mutant OSK1; it is >10000-fold more specific for this channel than for Kv1.1 and Kv1.2.



Voltage-gated potassium channel Kv1.3 has been shown to be a potential target for combating T cell-mediated autoimmune diseases, such as multiple sclerosis, type 1 diabetes, and rheumatoid arthritis.<sup>1–5</sup> In these diseases, terminally differentiated effector memory T cells express relatively higher levels of Kv1.3 channels and lower levels of calcium-activated potassium channels after activation.<sup>2,4</sup> Via the specific blocking of Kv1.3 channels, pristane-induced arthritis in rats can be ameliorated, and the incidence of experimental autoimmune diabetes in diabetes-prone rats can be reduced without causing significant side effects.<sup>4</sup> Thus, a potent and yet specific blocker of Kv1.3 could serve as a therapeutic agent for autoimmune diseases.

Various small compounds and polypeptides that block the Kv1.3 channel effectively have been reported. Of the small Kv1.3 blockers, 5-(4-phenoxybutoxy)psoralen (PAP-1), inhibiting Kv1.3 with a half-maximal effective concentration of 2 nM, is the most potent.<sup>6</sup> However, PAP-1 also effectively blocks other voltage-gated channels such as Kv1.1, Kv1.2, Kv1.4, Kv1.5, Kv1.6, and Kv1.7, limiting its pharmaceutical use. The specificity of PAP-1 for Kv1.3 over other Kv1.x channels is <50-fold.<sup>6</sup> High selectivity for Kv1.3 appears to be difficult to achieve for these small blockers,<sup>5</sup> possibly because the channel selectivity filter is highly conserved across voltage-gated potassium channels. In contrast, polypeptide blockers of Kv1.3 have been shown to have higher potency as well as better specificity for Kv1.3. For example, the K16D20 mutant of OSK1, a 38-residue toxin from the venom of the Asian scorpion *Orthochirus scrobiculosus*, blocks Kv1.3 with a half-maximal inhibitory concentration ( $IC_{50}$ ) of 0.003 nM, ~100-fold lower than those of Kv1.1 (0.4 nM) and Kv1.2 (3 nM), while it does

not block Kv1.4–Kv1.7 channels even at micromolar toxin concentrations.<sup>7,8</sup> ShK(L5), a synthetic analogue of ShK isolated from the sea anemone *Stichodactyla helianthus*, has also been shown to have >100-fold specificity for Kv1.3 ( $IC_{50}$  = 0.07 nM) versus other Kv1.x channels.<sup>3</sup> Replacing the Lys22 residue in ShK with diaminopropionic acid can increase the toxin's specificity for Kv1.3 ( $IC_{50}$  = 0.023 nM) over Kv1.1 ( $IC_{50}$  = 1.8 nM) to ~80-fold without reducing the potency for Kv1.3 significantly.<sup>9</sup> The derivatives ShK-170 and ShK-192 of ShK have been shown to inhibit Kv1.3 with an  $IC_{50}$  of 69–140 pM and >100-fold selectivity over other closely related channels.<sup>10</sup> A triple-point mutant of the kaliotoxin BmKTX (ADWX-1), inhibiting Kv1.3 with an  $IC_{50}$  of 0.002 nM, is ~300-fold specific for Kv1.3 over Kv1.1.<sup>11</sup> Therefore, mutants of available polypeptide toxins can be designed as potent and selective blockers of Kv1.3.

With an all-atom model of the bound complex by OSK1 and Kv1.3,<sup>12</sup> we are able to design a mutant OSK1, which we demonstrate to have improved potency and specificity for Kv1.3. In this mutant OSK1, the lysine residue at position 9 and the serine residue at position 11 are replaced with serine and arginine, respectively. Molecular dynamics (MD) simulations predict that S9R11 OSK1 blocks Kv1.3 with an  $IC_{50}$  of 0.2 pM, 1 order of magnitude more potent than the best blocker of Kv1.3 known previously.<sup>13</sup> The S9R11 OSK1 mutant not only shows promise for developing therapeutic agents but also

Received: December 8, 2011

Revised: January 10, 2012

Published: February 21, 2012

demonstrates how detailed intermolecular interactions can guide rational design of ion channel blockers.

## METHODS

**Initial Structures.** To examine the potency and specificity of S9R11 OSK1 for Kv1.3, we study the binding of the toxin to three channels belonging to the Kv1.x *Shaker* family, Kv1.1–Kv1.3. Other members of the Kv1.x family, including Kv1.4–Kv1.7, are not inhibited by OSK1 even at micromolar toxin concentrations<sup>7,8</sup> and therefore are not considered.

A homology model of Kv1.1 is generated using the crystal structure of Kv1.2 [Protein Data Bank (PDB) entry 3LUT]<sup>14,15</sup> as a template. The homology modeling method used is similar to that for Kv1.3 described previously.<sup>12</sup> The level of sequence identity between Kv1.1 (NCBI entry NP\_000208.2) and Kv1.2 is 93% in the pore domain. Structure 3LUT<sup>14,15</sup> and the homology model of Kv1.3 constructed previously<sup>12</sup> are used for Kv1.2 and Kv1.3, respectively. Kv1.1 and Kv1.2 are equilibrated in a POPC (2-oleoyl-1-palmitoyl-*sn*-glycero-3-phosphocholine) bilayer, solvated with explicit water and 0.2 M KCl with both the pore and the voltage sensor domain retained during the initial equilibration. During the equilibration, the P-loop turret of Kv1.1 and Kv1.2 moves substantially toward the voltage sensor domain by as much as 5–7 Å. The equilibrated channels are then symmetrized and truncated for subsequent molecular docking calculations and umbrella sampling, to provide the required degree of computational efficiency. After truncation, only transmembrane domains S5 and S6 forming the pore domain are retained. This truncation does not affect the ability of the channels to bind the toxins significantly, as demonstrated previously.<sup>12</sup> Nuclear magnetic resonance structure 1SCO<sup>16</sup> is used for OSK1. The structure of the mutant OSK1 is generated by replacing the side chains of residues K9 and S11 of OSK1 with S and R, respectively, in VMD version 1.9.<sup>17</sup>

The bound states of both the wild-type and mutant OSK1 with the three truncated channels are predicted using the rigid-body molecular docking program ZDOCK version 3.0.1.<sup>18</sup> In each case, 600 channel–toxin structures are generated. Of the 600 channel–toxin structures generated in each case, we selected one complex that is most consistent with the experimental findings. Thus, we consider only those docking complexes in which the lysine residue at position 27 protrudes into the selectivity filter of the channel.<sup>19</sup> Less than 3% of the complexes generated by the ZDOCK program meet this criterion, and these are not among the top ranked. This highlights the inadequacy of rigid-body docking algorithms in predicting toxin–channel complexes without existing knowledge. The highest ranked of the complexes in which Lys27 of the toxin is docked into the selectivity filter is selected for subsequent MD simulations. For each selected toxin–channel complex, a rectangular simulation box is constructed in which the complex is embedded in a POPC bilayer solvated with explicit water and 0.2 M KCl. Two bulk K<sup>+</sup> ions are presented in the S2 and S4 binding sites of the channel selectivity filter, while the S0 binding site is expected to be occupied by the side chain of the Lys27 residue of the toxins. The systems are energy minimized and further equilibrated for 3.5–5.0 ns, during which the channel backbone atoms and the two K<sup>+</sup> ions in the selectivity filter are restrained to the initial structure by a force constant of 0.25 kcal mol<sup>-1</sup> Å<sup>-2</sup>. The toxin backbone is free to move throughout the simulation. The MD simulations allow the toxin–channel complexes to evolve such that the most favorable interactions are formed. For example, Figure S1 of the

Supporting Information demonstrates that OSK1 rotates along the channel axis during the simulation, and a salt bridge is finally formed between Arg24 of OSK1 and Asp433 of Kv1.3.

**Molecular Dynamics (MD) Simulations.** All MD simulations are performed using NAMD version 2.7.<sup>20</sup> The CHARMM27/CMAP force fields for proteins and lipids<sup>21–24</sup> and the TIP3P model for water<sup>25</sup> are used. The switch and cutoff distances for short-range interactions are set to 8.0 and 12.0 Å, respectively. The particle mesh Ewald method<sup>26</sup> is used to describe long-range electrostatic interactions, with a maximal grid spacing of 1.0 Å. Rectangular periodic boundary conditions are applied. The SHAKE<sup>27</sup> and SETTLE<sup>28</sup> algorithms are used to keep the bond lengths in the system rigid, allowing a time step of 2 fs to be used. The short-range nonbonded interactions are computed every step, while the long-range electrostatic forces are evaluated every two steps together with the pair list. In all simulations, the temperature is kept constant at an average value of 300 K using Langevin dynamics with a damping coefficient of 1 ps<sup>-1</sup>. The Nosé–Hoover Langevin piston method<sup>29</sup> is used to maintain the pressure in the system at an average value of 1 atm, with the barostat oscillation and damping time scales set to 200 and 100 ps, respectively. The pressure coupling is semiisotropic. Trajectories are saved every 20 ps for analysis.

**Umbrella Sampling.** We use umbrella sampling to construct a one-dimensional PMF for the unbinding of the toxin along the channel axis, which allows the IC<sub>50</sub> for the toxin block to be calculated rigorously.<sup>30</sup> Umbrella sampling represents one of the most efficient methods for reliably deriving the PMF for complex ligands such as the polypeptide toxins examined in this work, as demonstrated by Kuyucak and co-workers.<sup>31,32</sup> The equilibrated toxin–channel complexes are used to generate umbrella windows, spaced at 0.5 Å intervals. A force of 20 or 30 kcal mol<sup>-1</sup> Å<sup>-1</sup> is applied to pull the toxin out of the binding site. During the pulling, a harmonic restraint is applied to maintain a rigid toxin backbone. The umbrella sampling reaction coordinate is the channel permeation pathway (*z* dimension), which is parallel to the bilayer normal.

A force constant of 20–40 kcal mol<sup>-1</sup> Å<sup>-2</sup>, depending on the channel and the position of the umbrella window, is used to restrain the center of mass (COM) of the backbone atoms of the toxin to the center of each umbrella window. The COM of the toxin is confined to a cylinder with a radius of 8 Å centered on the channel axis, with a flat-bottom harmonic potential of 20 kcal mol<sup>-1</sup> Å<sup>-2</sup>. This radius of 8 Å ensures that the cylindrical restraint potential is always zero when the toxin is bound, so that the toxin is allowed to rotate and move freely. Each umbrella window is simulated for at least 5 ns. The depth of the profiles of the potential of mean force (PMF) changes by <0.5 *kT* over the last 1 ns, and thus, we assume convergence. The channel is free to move during umbrella sampling, with the exception of the acidic residues of the P-loop turret of Kv1.1 and Kv1.2, whose backbones are restrained to the initial position using a harmonic potential with a force constant of 1 kcal mol<sup>-1</sup> Å<sup>-2</sup>. The COM coordinates of the backbone atoms of the toxins along the *z* dimension are saved every 1 ps for analysis.

**Data Analysis.** The PMF profile is constructed with the weighted histogram analysis method.<sup>33</sup> The PMF value of the window at *z* = 45 Å, assumed to be similar to the bulk, is set to zero. Note that the COM for the channel is *z* = 0 Å. The first 1 ns of each window is considered as equilibration and not included in the calculations of the PMF. The IC<sub>50</sub>, defined as

the concentration of the toxin at which the probability of the channel being blocked is 0.5 in molar units, is estimated as

$$IC_{50}^{-1} = 1000\pi R^2 N_A \int_{z_{\min}}^{z_{\max}} \exp[-W(z)/kT] dz \quad (1)$$

where  $R$  equals 8 Å,  $N_A$  is Avogadro's number,  $z_{\min}$  and  $z_{\max}$  are the boundaries of the binding site along the channel axis,  $W(z)$  is the PMF at the window  $z$ , and  $kT$  assumes the usual significance. We note that  $W(z)$  is dependent on the choice of  $R$ , whereas  $IC_{50}$  is independent of  $R$ .<sup>34</sup> The electrostatic interaction energy is calculated according to the potential energy function of the CHARMM force field.<sup>23</sup>

## RESULTS AND DISCUSSION

### Binding Affinities of Pore Blockers Can Be Reliably Predicted.

We show that the binding affinities derived from computational studies closely match those determined experimentally. Using a molecular docking method and MD simulations, we first determine the binding modes of three toxins, namely, charybdotoxin (ChTX), ShK, and OSK1, with respect to the Kv1.3 channel.<sup>12</sup> We then construct, using MD simulations and umbrella sampling, the PMF profiles for each of these three polypeptide toxins as they are progressively pulled away from the channel–toxin complexes. From the PMF profiles computed, we estimate the binding affinity, specifically,  $IC_{50}$ , of each toxin for the channel. The  $IC_{50}$  values predicted from our PMF calculations are 25.3, 0.17, and 0.02 nM for ChTX, ShK, and OSK1, respectively.<sup>12</sup> The values determined experimentally for the three toxins are 0.7–2.6,<sup>35,36</sup> 0.01,<sup>9</sup> and 0.014 nM, respectively.<sup>8</sup> Thus, the  $IC_{50}$  value calculated from the PMF profile for OSK1 is in accord with that measured experimentally. One of the largest discrepancies we found occurs with ChTX, for which the measured and computed  $IC_{50}$  values differ by ~1 order of magnitude. The depth of the PMF profile for this toxin is slightly underestimated possibly because of an unstable contact between an acidic residue in the channel (Glu420) and a basic residue in the toxin (Arg25) during the sampling period of 5 ns.

**S9R11 OSK1 Is Potent for Kv1.3.** The bound complex between Kv1.3 and OSK1 after 3.5 ns of MD equilibration reveals that an arginine residue from the toxin makes a firm contact with an acidic residue on the channel wall, just outside of the selectivity filter, while the side chain of another lysine residue is lodged into the selectivity filter. These interactions, together with several other transient hydrogen bonds formed between the ellipsoidal ligand and the vestibule, render the channel highly sensitive to the polypeptide toxin. Detailed interactions between OSK1 and Kv1.3 have been described previously.<sup>12</sup> There is, however, one unfavorable electrostatic interaction in the channel–toxin complex. As shown in Figure 1, a basic residue (Lys458) lining the wall of the external vestibule faces another basic residue (Lys9) of OSK1, causing a Coulomb repulsion. Figure S2 of the Supporting Information shows that the distance between the side chain nitrogen atoms of Lys9 and Lys458 fluctuates between 4 and 9 Å over the last 1.5 ns of the equilibration. Positioned adjacent to Lys458 is an acidic residue (Asp449) of Kv1.3, which faces a serine residue (Ser11) of the toxin. We reasoned that the binding affinity of the toxin for Kv1.3 could be made to increase appreciably if the positions of the two amino acids in the toxin were interchanged. To test this idea, we first placed an arginine at position 11, which normally is occupied by a serine (S11R

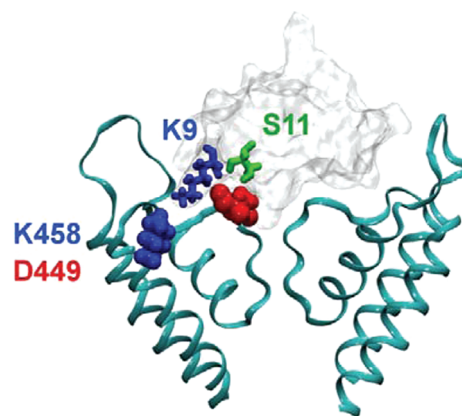


**Figure 1.** OSK1 bound to the Kv1.3 channel after 3.5 ns of MD simulation showing two toxin–channel contacts, K9–K458 and S11–D449. The OSK1 surface is shown in transparent silver. Two channel subunits are colored cyan.

mutation), and a serine at position 9, which normally is occupied by a lysine (K9S mutation). Here, mutation of Lys9 to an acidic residue is not considered, because the outer vestibular wall of Kv1.3 contains several rings of acidic residues. With this interchange, Asp449 is now facing an arginine and Lys458 is facing a neutral and yet polar serine residue. From simple electrostatic considerations, we would expect the double mutant toxin, [K9S]-[S11R]-OSK1, to have an enhanced sensitivity to Kv1.3, compared to that of wild-type OSK1.

Consistent with this expectation, the  $IC_{50}$  of the toxin for Kv1.3, as determined by the depth of the PMF profile, is greatly reduced when the positions of the two residues, Ser9 and Lys11, are interchanged. As shown in Figure 2, the minima of

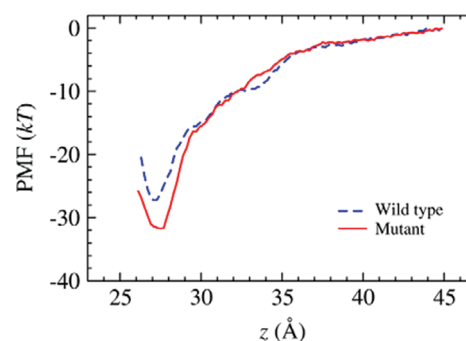


**Figure 2.** PMF profiles for the unbinding of wild-type and S9R11 mutant OSK1 from Kv1.3.

the PMF profiles obtained from the wild-type and mutant OSK1 are  $-27.2$  and  $-31.8$   $kT$ , respectively. The energy minima are at  $z = 27\text{--}28$  Å, relative to the center of mass of the channel, which is at  $z = 0$  Å. The predicted  $IC_{50}$  value for the wild-type toxin is 20 pM, which is close to the experimental value of 14 pM.<sup>7</sup> The mutant toxin blocks Kv1.3 with a predicted  $IC_{50}$  value of 0.2 pM. Thus, the two mutations on the toxin, K9S and S11R, increase the potency of OSK1 for Kv1.3 by 100-fold. The predicted  $IC_{50}$  of the mutant toxin is 1 order of magnitude lower than that of the most potent blocker of this channel thus far identified (ADWX-1, for which  $IC_{50} = 2$  pM<sup>11</sup>).

**S9R11 OSK1 Is Selective for Kv1.3.** One of the objectives of many previous studies of Kv1.3 has been to identify

compounds that show high sensitivity and selectivity for this channel.<sup>3,7–9,13</sup> To determine the specificity of the mutant OSK1 for Kv1.3, we construct PMF profiles for the dissociation of the wild-type and mutant OSK1 from Kv1.1 and Kv1.2.

Voltage-gated K<sup>+</sup> channels contain a typically unstructured loop at the outer vestibule of the channel linking the S5 pore-forming helix and the selectivity filter, commonly termed the P-loop turret. Unlike the highly conserved selectivity filter, the primary sequence of the turret varies significantly between channels. For Kv1.1–Kv1.3 channels, the turret is abundant in acidic residues. An alignment of the primary sequence of the turret of these three channels is given in Figure 3c. The first

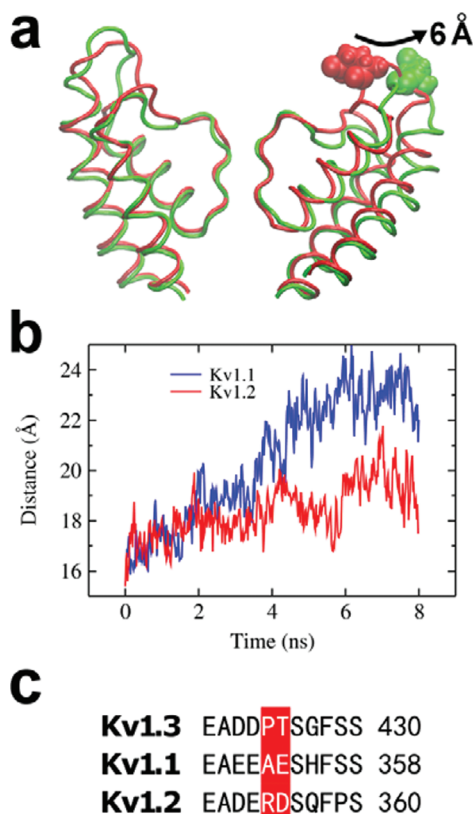


**Figure 3.** (a) Pore domain of the Kv1.1 channel before (red) and after (green) 8 ns of unrestrained simulation. Atoms of residue Glu353 in one channel subunit are shown as spheres. Two channel subunits are shown. (b) Maximal distance between the center of mass of the backbone atoms of residues Glu353 of Kv1.1 and Asp355 of Kv1.2 and the channel central axis as a function of simulation time. (c) Sequence alignment of the P-loop turret of channels Kv1.1–Kv1.3.

three acidic residues are conserved across the three channels, while Kv1.1 and Kv1.2 have an additional aspartate or glutamate residue at the center of the turret. The three conserved acidic residues are directly linked to the S5 transmembrane helix. Therefore, the movement of these three residues is limited. In contrast, the acidic residue at the middle of the turret of Kv1.1 and Kv1.2 is free to move in response to external interactions, such as attraction from the basic residues in the S4 voltage sensing helix. Experimentally, it has been suggested that the P-loop turret can largely account for the specificity of toxin ADWX-1 for Kv1.3 over Kv1.1.<sup>11</sup> Thus, to predict the toxin binding affinity accurately, the position of the turret must be correctly modeled. To determine the most appropriate location of the turret in Kv1.1 and Kv1.2,

the two channels are equilibrated with the voltage sensing helix S4 retained before truncation for subsequent molecular docking and MD simulations.

Figure 3a illustrates that the turret of one subunit of Kv1.1 moves substantially in the presence of the voltage sensing helix S4. In particular, the distance from residue Glu353 of Kv1.1 to the channel central axis increases by up to  $\sim 7$  Å after equilibration for 8 ns in the presence of the S4 helix (Figure 3b). We observe that each of the four turrets moves independently and becomes displaced laterally by a different distance during the simulation period of 8 ns. It is likely that in reality each turret undergoes fluctuations from its mean position, the maximal movement we observe representing the outermost position the turret occupies. Similarly, Asp355 of Kv1.2 also becomes laterally displaced in the presence of the S4 helix, albeit to a lesser extent than that observed for Kv1.1 (Figure 3b). The movement of the turret toward the S4 helix observed for Kv1.1 and Kv1.2 is apparently due to the additional negative charge at the center of their turrets (Glu353 of Kv1.1 and Asp355 of Kv1.2), which is attracted by the basic residues of the S4 helix. Asp355 of Kv1.2 moves less significantly within the time scale of the simulation, possibly because the adjacent Arg354 residue is repelled by the S4 helix or the turret of Kv1.2 is more rigid than that of Kv1.1.

Given that the positions of the turrets of Kv1.1 and Kv1.2 are dependent on the presence or absence of the S4 helix, the PMF profiles should ideally be constructed with this helix in place. Such calculations, however, become prohibitively computationally expensive. Thus, in subsequent MD simulations and umbrella sampling, the S4 helix of Kv1.1 and Kv1.2 is truncated, and the turrets are placed at what we observe to be their mean positions. Harmonic restraints are then applied to maintain the distance between the center of mass of the backbone atoms of residue Glu353 of Kv1.1 and the channel axis in the range of  $21.0 \pm 1.5$  Å, corresponding to an intermediate range observed during the 8 ns equilibration. Similarly, the distance between the center of mass of the backbone atoms of Asp355 of Kv1.2 is also harmonically restrained to be around an average value of 20.0 Å, 1 Å lower than that of Kv1.1. We show below that with the appropriate restraint applied the IC<sub>50</sub> values for the binding of wild-type OSK1 to both Kv1.1 and Kv1.2 channels can be predicted with a fair degree of accuracy.

Table 1 shows the IC<sub>50</sub> values calculated from the PMF profiles for the wild-type and mutant OSK1. Experimentally

**Table 1. Predicted IC<sub>50</sub> Values for Wild-Type and S9R11 Mutant OSK1 Inhibiting Kv1.1–Kv1.3 Channels<sup>a</sup>**

channel	IC <sub>50</sub> (nM)	
	OSK1	S9R11 OSK1
Kv1.1	0.2 (0.6)	30
Kv1.2	63 (5.6)	45
Kv1.3	0.02 (0.014)	0.0002

<sup>a</sup>Numbers in parentheses are corresponding experimental values for wild-type OSK1 obtained by Mouhat et al.<sup>7</sup>

determined values for wild-type OSK1 are given in parentheses. For comparison, the IC<sub>50</sub> values for Kv1.3 are also given. The results demonstrate that the mutant OSK1 has a specificity of >10000-fold for Kv1.3 over Kv1.1 and Kv1.2.

**Structural Basis for Potency and Selectivity.** The exquisite potency of the mutant OSK1 with respect to Kv1.3, as well as its selectivity for this channel over Kv1.1 and Kv1.2,

results from the different amino acid compositions of the turrets and the locations of acidic and basic residues in the external vestibule. The snapshots of the toxin–channel complexes for Kv1.3, shown in Figure 4, are selected after

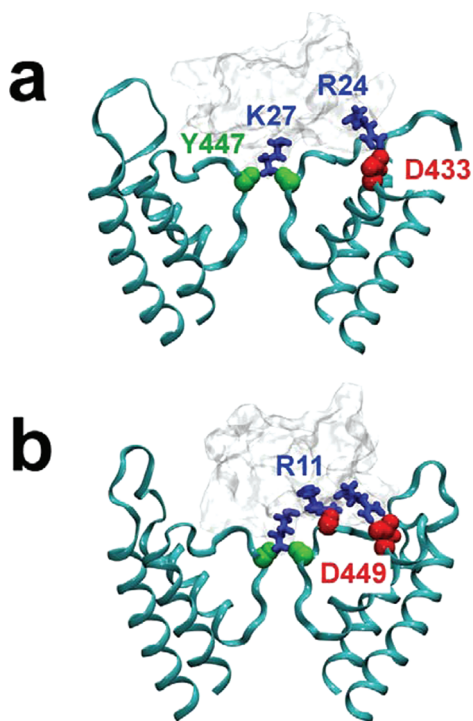


**Figure 4.** Wild-type OSK1 (a) and S9R11 mutant OSK1 (b) bound to the Kv1.3 channel. The toxin surface is shown in transparent silver. Two channel subunits are shown as cyan ribbons.

the equilibration period of 5 ns with molecular dynamics simulations. The important residue pairs for the binding of the toxin to Kv1.3 are highlighted. The wild-type and mutant toxins form hydrogen bonds between the side chain of toxin residue Lys27 and the carbonyl group of Tyr447 of the channel selectivity filter, as indicated in Figure 4. The Arg24 residues of both toxins also form hydrogen bonds with the Asp433 residue, located just outside of the selectivity filter. With the mutant toxin, we also see another pair of toxin and channel residues interacting, as indicated in Figure 4b. Arg11, which in the wild-type toxin is a serine, is in contact with Asp449, which is near the pore entrance,  $\sim 8$  Å from the selectivity filter. The side chain of the Arg11 residue is fully extended, forming hydrogen bonds and salt bridges with the acidic Asp449 residue. The electrostatic interaction energy between the two residues is now  $-45.2$  kcal/mol. Moreover, the serine residue at position 9 of the mutant toxin interacts only weakly with the Lys458 residue of the channel, with an interaction energy of 4.3 kcal/mol. In the wild-type toxin, this position is occupied by another lysine; the Coulomb repulsion between the interacting residues gives rise to an interaction energy of 25.6 kcal/mol and causes the side chain of Lys9 to bend away from the channel wall. The toxin is thus made to bind much more firmly to Kv1.3 with these two amino acid substitutions, compared to that of its original form.

In the case of Kv1.1 and Kv1.2, the negative charge at the center of the P-loop turret (Glu353 of Kv1.1 and Asp355 of Kv1.2) appears to attract the toxin from the binding site, causing the toxin to bind more shallowly in the channel

selectivity filter. This is reflected in the less negative electrostatic interaction energy between the Lys27 residue of the toxin and a tyrosine residue in the channel selectivity filter, which form one of the two firm contacts between the toxin and the channel. The electrostatic interaction of this contact is significantly weaker for Kv1.1 and Kv1.2 than for Kv1.3 (see Table 2), consistent with wild-type OSK1 being less potent

**Table 2. Electrostatic Interaction Energies (kilocalories per mole) between Toxin–Channel Residue Pairs for OSK1 and Its S9R11 Mutant<sup>a</sup>**

channel	residue pair <sup>b</sup>	wild type	mutant
Kv1.3	K27–Y447	−73.3	−72.1
	R24–D433	−78.2	−93.6
	K(S)9–K458	25.6	4.3
	S(R)11–D449	−7.2	−45.2
Kv1.1	K27–Y375	−56.3	−63.5
	R24–D361	−90.3	−11.5
	K(S)9–K386	1.0	−0.6
	S(R)11–D377	−8.1	−32.8
Kv1.2	K27–Y377	−50.0	−68.7
	R12–D363	−88.9	−6.03
	K(S)9–K388	10.8	1.5
	S(R)11–D379	−9.3	−80.8

<sup>a</sup>The standard error of the mean is  $<2$  kcal/mol in all cases.

<sup>b</sup>Characters in parentheses indicate corresponding residues of the mutant OSK1.

with respect to Kv1.1 and Kv1.2 than with respect to Kv1.3 (Table 1).

In Table 2, we list the electrostatic energies of four interacting residue pairs between the wild-type and mutant toxins and Kv1.1–Kv1.3. Although the total electrostatic interaction energies are not generally correlated with the binding affinities, it is nevertheless instructive to examine how the strengths of several pairwise electrostatic interactions change after the mutation of the toxin. Table 2 shows that the mutation causes OSK1 to form an extra electrostatic contact with a channel aspartate residue at the pore entrance of Kv1.1 (Asp377) and Kv1.2 (Asp379). However, the mutation also causes another firm toxin–channel contact to break for these two channels. Specifically, the hydrogen bonds formed by Arg24 of the wild-type toxin and Asp361 of Kv1.1 are not present in the bound complex between the mutant toxin and the channel (see Table S1 of the Supporting Information). Thus, the mutation does not significantly increase the potency of OSK1 with respect to Kv1.1 and Kv1.2. In particular, as shown in Table 1, the mutant OSK1 appears to be  $\sim 150$ -fold less potent with respect to Kv1.1.

## CONCLUDING REMARKS

Many polypeptide toxins extracted from scorpion venoms exhibit a similar structural motif and block families of voltage-gated potassium (Kv) channels. Typically, these toxins, including OSK1, have a triple- or quadruple-stranded antiparallel  $\beta$ -sheet and a short helix interconnected by three disulfides. The polypeptides comprising 25–45 amino acid residues are tightly packed by disulfide bridges, which confer their structural rigidity. Because these peptides block Kv channels with high potency, they can potentially serve as prototypes for the design of modern drugs targeting several types of biological ion channels. The toxins, however, have

evolved to act on a broad spectrum of channels for rapid paralysis of prey, rather than to be highly selective to a specific channel type. Also, their large mass and the abundance of hydrophilic amino acid residues may prevent them from crossing epithelia, including the blood–brain barrier.

Attempts have been made to reduce the size of the polypeptide by pruning the terminal domains of OSK1<sup>7</sup> or the loop in  $\alpha$ -conotoxin,<sup>37</sup> a potent blocker of  $\alpha 7$  nicotinic acetylcholine receptor, and test their affinity and conformational stability. Also, numerous studies have been conducted to determine the changes in toxin affinity and selectivity following site-directed mutagenesis.<sup>3,9,13</sup> Because of the lack of availability of atomic details about the channel–toxin complexes, such theoretical as well as experimental mutations in the past have been largely guided by intuition and careful reasoning. Nevertheless, many useful insights have been gleaned about the mechanisms of blocking by scorpion toxins, and the key amino acid residues in the polypeptide interacting with the binding sites in the external vestibules of Kv channels have been identified.

In this study, we demonstrate, at the proof-of-principle level, how computational tools can be used to conduct theoretical site-directed mutagenesis to improve the potency and selectivity of polypeptide blockers of ion channels. From the OSK1–Kv1.3 complex formed from MD simulations, we have identified two residues, the mutation of which would provide an enhanced binding affinity. The mutant OSK1 we devised has an IC<sub>50</sub> value of 0.2 pM and a specificity of >10000-fold for Kv1.3 versus Kv1.1 and Kv1.2. Thus, one possible approach for developing drugs targeting autoimmune diseases mediated by human T cells is to use a potent scorpion toxin, such as the mutant OSK1, as a structural template and to successively prune it such that the spatial arrangement of the bioactive amino acids remains unchanged. Alternatively, new blockers may possibly be developed from small molecules, one of whose side chains protrudes into the selectivity filter, by incrementally adding new groups to it to form several drug–channel interacting pairs, similar to those found in the mutant OSK1–Kv1.3 complex. For such strategies to be successful, it is desirable to devise a computational method that can rapidly and reliably screen a large number of lead candidates. Once such a technique becomes available, theoretical approaches for studying ligand–channel complexes may play an important role in the rational development of drugs.

## ■ ASSOCIATED CONTENT

### ● Supporting Information

Two figures and one table. This material is available free of charge via the Internet at <http://pubs.acs.org>.

## ■ AUTHOR INFORMATION

### Corresponding Author

\*Research School of Biology, Australian National University, Canberra, ACT 0200, Australia. Telephone: +61-2-6125-4337. Fax: +61-2-6125-0739. E-mail: [rong.chen@anu.edu.au](mailto:rong.chen@anu.edu.au).

### Funding

This research was undertaken on the NCI National Facility in Canberra, Australia, which is supported by the Australian Commonwealth Government.

## ■ ABBREVIATIONS

COM, center of mass; MD, molecular dynamics; PMF, potential of mean force.

## ■ REFERENCES

- (1) Crest, M., Beraud-Juven, E., and Gola, M. (1999) Towards therapeutic applications of Kv1 channel blockers in neurological diseases. *Perspect. Drug Discovery* 16, 333–342.
- (2) Wulff, H., Calabresi, P. A., Allie, R., Yun, S., Pennington, M., Beeton, C., and Chandy, K. G. (2003) The voltage-gated Kv1.3 K<sup>+</sup> channel in effector memory T cells as new target for MS. *J. Clin. Invest.* 111, 1703–1713.
- (3) Beeton, C., Pennington, M. W., Wulff, H., Singh, S., Nugent, D., Crossley, G., Khaytin, I., Calabresi, P. A., Chen, C. Y., Gutman, G. A., and Chandy, K. G. (2005) Targeting effector memory T cells with a selective peptide inhibitor of Kv1.3 channels for therapy of autoimmune diseases. *Mol. Pharmacol.* 67, 1369–1381.
- (4) Beeton, C., Wulff, H., Standifer, N. E., Azam, P., Mullen, K. M., Pennington, M. W., Kolski-Andreaco, A., Wei, E., Grino, A., Counts, D. R., Wang, P. H., LeeHealey, C. J., Andrews, B. S., Sankaranarayanan, A., Homerick, D., Roeck, W. W., Tehranzadeh, J., Stanhope, K. L., Zimin, P., Havel, P. J., Griffey, S., Knaus, H. G., Nepom, G. T., Gutman, G. A., Calabresi, P. A., and Chandy, K. G. (2006) Kv1.3 channels are a therapeutic target for T cell-mediated autoimmune diseases. *Proc. Natl. Acad. Sci. U.S.A.* 103, 17414–17419.
- (5) Wulff, H., Castle, N. A., and Pardo, L. A. (2009) Voltage-gated potassium channels as therapeutic targets. *Nat. Rev. Drug Discovery* 8, 982–1001.
- (6) Schmitz, A., Sankaranarayanan, A., Azam, P., Schmidt-Lassen, K., Homerick, D., Hänsel, W., and Wulff, H. (2005) Design of PAP-1, a selective small molecule Kv1.3 blocker, for the suppression of effector memory T cells in autoimmune diseases. *Mol. Pharmacol.* 68, 1254–1270.
- (7) Mouhat, S., Visan, V., Ananthakrishnan, S., Wulff, H., Andreotti, N., Grissmer, S., Darbon, H., De Waard, M., and Sabatier, J.-M. (2005) K<sup>+</sup> channel types targeted by synthetic OSK1, a toxin from *Orthochirus scrobiculosus* scorpion venom. *Biochem. J.* 385, 95–104.
- (8) Mouhat, S., Teodorescu, G., Homerick, D., Visan, V., Wulff, H., Wu, Y., Grissmer, S., Darbon, H., De Waard, M., and Sabatier, J.-M. (2006) Pharmacological profiling of *Orthochirus scrobiculosus* toxin 1 analogs with a trimmed N-terminal domain. *Mol. Pharmacol.* 69, 354–362.
- (9) Kalman, K., Pennington, M. W., Lanigan, M. D., Nguyen, A., Rauer, H., Mahnir, V., Paschetto, K., Kem, W. R., Grissmer, S., Gutman, G. A., Christian, E. P., Cahalan, M. D., Norton, R. S., and Chandy, K. G. (1998) ShK-Dap<sup>22</sup>, a potent Kv1.3-specific immunosuppressive polypeptide. *J. Biol. Chem.* 273, 32697–32707.
- (10) Pennington, M. W., Beeton, C., Galea, C. A., Smith, B. J., Chi, V., Monaghan, K. P., Garcia, A., Rangaraju, S., Giuffrida, A., Plank, D., Crossley, G., Nugent, D., Khaytin, I., Lefievre, Y., Peshenko, I., Dixon, C., Chauhan, S., Orzel, A., Inoue, T., Hu, X., Moore, R. V., Norton, R. S., and Chandy, K. G. (2009) Engineering a stable and selective peptide blocker of the Kv1.3 channel in T lymphocytes. *Mol. Pharmacol.* 75, 762–773.
- (11) Yin, S. J., Jiang, L., Yi, H., Han, S., Yang, D. W., Liu, M. L., Liu, H., Cao, Z. J., Wu, Y. L., and Li, W. X. (2008) Different residues in channel turret determining the selectivity of ADWX-1 inhibitor peptide between Kv1.1 and Kv1.3 channels. *J. Proteome Res.* 7, 4890–4897.
- (12) Chen, R., Robinson, A., Gordon, D., and Chung, S. H. (2011) Modeling the binding of three toxins to the voltage-gated potassium channel (Kv1.3). *Biophys. J.* 101, 2652–2660.
- (13) Han, S., Yi, H., Yin, S. J., Chen, Z. Y., Liu, H., Cao, Z. J., Wu, Y. L., and Li, W. X. (2008) Structural basis of a potent peptide inhibitor designed for Kv1.3 channel, a therapeutic target of autoimmune disease. *J. Biol. Chem.* 283, 19058–19065.

- (14) Long, S. B., Campbell, E. B., and Mackinnon, R. (2005) Voltage sensor of Kv1.2: Structural basis of electromechanical coupling. *Science* 309, 903–908.
- (15) Chen, X., Wang, Q., Ni, F., and Ma, J. (2010) Structure of the full-length Shaker potassium channel Kv1.2 by normal-mode-based X-ray crystallographic refinement. *Proc. Natl. Acad. Sci. U.S.A.* 107, 11352–11357.
- (16) Jaravine, V. A., Nolde, D. E., Reibarkh, M. J., Korolkova, Y. V., Kozlov, S. A., Pluzhnikov, K. A., Grishin, E. V., and Arseniev, A. S. (1997) Three-dimensional structure of toxin OSK1 from *Orthochirus scrobiculosus* scorpion venom. *Biochemistry* 36, 1223–1232.
- (17) Humphrey, W., Dalke, A., and Schulten, K. (1996) VMD: Visual molecular dynamics. *J. Mol. Graphics* 14, 33–38.
- (18) Mintseris, J., Pierce, B., Wiehe, K., Anderson, R., Chen, R., and Weng, Z. (2007) Integrating statistical pair potentials into protein complex prediction. *Proteins* 69, 511–520.
- (19) Lange, A., Giller, K., Hornig, S., Martin-Eauclaire, M. F., Pongs, O., Becker, S., and Baldus, M. (2006) Toxin-induced conformational changes in a potassium channel revealed by solid-state NMR. *Nature* 440, 959–962.
- (20) Phillips, J. C., Braun, R., Wang, W., Gumbart, J., Tajkhorshid, E., Villa, E., Chipot, C., Skeel, R. D., Kalé, L., and Schulten, K. (2005) Scalable molecular dynamics with NAMD. *J. Comput. Chem.* 26, 1781–1802.
- (21) Feller, S. E., Gawrisch, K., and MacKerell, A. D. (2002) Polyunsaturated fatty acids in lipid bilayers: Intrinsic and environmental contributions to their unique physical properties. *J. Am. Chem. Soc.* 124, 318–326.
- (22) Feller, S. E., and MacKerell, A. D. (2000) An improved empirical potential energy function for molecular simulations of phospholipids. *J. Phys. Chem. B* 104, 7510–7515.
- (23) MacKerell, A. D., Bashford, D., Bellott, M., Dunbrack, R. L., Evansck, J. D., Field, M. J., Fischer, S., Gao, J., Guo, H., Ha, S., Joseph-McCarthy, D., Kuchnir, L., Kuczera, K., Lau, F. T. K., Mattos, C., Michnick, S., Ngo, T., Nguyen, D. T., Prodhom, B., Reiher, W. E., Roux, B., Schlenkrich, M., Smith, J. C., Stote, R., Straub, J., Watanabe, M., Wiórkiewicz-Kuczera, J., Yin, D., and Karplus, M. (1998) All-atom empirical potential for molecular modeling and dynamics studies of proteins. *J. Phys. Chem. B* 102, 3586–3616.
- (24) MacKerell, A. D., Feig, M., and Brooks, C. L. (2004) Extending the treatment of backbone energetics in protein force fields: Limitations of gas-phase quantum mechanics in reproducing protein conformational distributions in molecular dynamics simulations. *J. Comput. Chem.* 25, 1400–1415.
- (25) Jorgensen, W. L., Chandrasekhar, J., Madura, J. D., Impey, R. W., and Klein, M. L. (1982) Comparison of simple potential functions for simulating liquid water. *J. Chem. Phys.* 79, 926–935.
- (26) Darden, T., York, D., and Pedersen, L. (1993) Particle mesh Ewald: An  $N \cdot \log(N)$  method for Ewald sums in large systems. *J. Chem. Phys.* 12, 10089.
- (27) Ryckaert, J. P., Ciccotti, G., and Berendsen, H. J. C. (1977) Numerical integration of the Cartesian equations of motion of a system with constraints: Molecular dynamics of  $n$ -alkanes. *J. Comput. Phys.* 23, 327–341.
- (28) Miyamoto, S., and Kollman, P. A. (1992) SETTLE: An analytical version of the SHAKE and RATTLE algorithm for rigid water models. *J. Comput. Chem.* 13, 952–962.
- (29) Martyna, G. J., Tobias, D. J., and Klein, M. L. (1994) Constant pressure molecular dynamics algorithms. *J. Chem. Phys.* 101, 4177–4189.
- (30) Allen, T. W., Andersen, O. S., and Roux, B. (2004) Energetics of ion conduction through the gramicidin channel. *Proc. Natl. Acad. Sci. U.S.A.* 101, 117–122.
- (31) Baştuğ, T., Chen, P. C., Patra, S. M., and Kuyucak, S. (2008) Potential of mean force calculations of ligand binding to ion channels from Jarzynski's equality and umbrella sampling. *J. Chem. Phys.* 128, 155104.
- (32) Chen, P. C., and Kuyucak, S. (2011) Accurate determination of the binding free energy for KcsA-charybdotoxin complex from the potential of mean force calculations with restraints. *Biophys. J.* 100, 2466–2474.
- (33) Kumar, S., Bouzida, D., Swendsen, R. H., Kollman, P. A., and Rosenberg, J. M. (1992) The weighted histogram analysis method for free-energy calculations on biomolecules. I. The method. *J. Comput. Chem.* 13, 1011–1021.
- (34) Roux, B., Andersen, O., and Allen, T. W. (2008) Comment on “Free energy simulations of single and double ion occupancy in gramicidin A” [ *J. Chem. Phys.* 126, 105103 (2007) ]. *J. Chem. Phys.* 128, 227101.
- (35) Grissmer, S., Nguyen, A. N., Aiyar, J., Hanson, D. C., Mather, R. J., Gutman, G. A., Karmilowicz, M. J., Auperin, D. D., and Chandy, K. G. (1994) Pharmacological characterization of five cloned voltage-gated  $K^+$  channels, types Kv1.1, 1.2, 1.3, 1.5, and 3.1, stably expressed in mammalian cell lines. *Mol. Pharmacol.* 45, 1227–1234.
- (36) Aiyar, J., Withka, J. M., Rizzi, J. P., Singleton, D. H., Andrews, G. C., Lin, W., Boyd, J., Hanson, D. C., Simon, M., Dethlefs, B., Lee, C., Hall, J. E., Gutman, G. A., and Chandy, K. G. (1995) Topology of the pore-region of a  $K^+$  channel revealed by the NMR-derived structures of scorpion toxins. *Neuron* 15, 1169–1181.
- (37) Jin, A. H., Daly, N. L., Nevin, S. T., Wang, C. I., Dutertre, S., Lewis, R. J., Adams, D. J., Craik, D. J., and Alewood, P. F. (2008) Molecular engineering of conotoxins: The importance of loop size to  $\alpha$ -conotoxin structure and function. *J. Med. Chem.* 51, 5575–5584.